

UNIVERSITY OF ZURICH

# Comparison of Measured and Simulated Light Yield in Plastic Scintillators

by

Markus Baumgartner

Bachelor-Thesis  
Supervisor  
Prof. Dr. Ulrich Straumann  
Roman Gredig

in the  
Faculty of Science  
Physik-Institut

November 2013

*"No. Try not. Do... or do not. There is no try."*

Master Yoda

UNIVERSITY OF ZURICH

*Abstract*

Faculty of Science  
Physik-Institut

Bachelor-Thesis

by Markus Baumgartner

We present the results of experimental studies on the physical coherency of the fibre simulation tool-kit for the Mu3e experiment developed with Geant4 [1]. The goal was to investigate different aspects of the simulation i.e. surface properties and wrapping and to check the simulation for overall comparable results with the experimental setup. To achieve this the simulation was modified in different aspects to match the experimental setup i.e. geometry of the scintillation material, scintillating and optical properties of the experiment. Different simulations were carried out and the results compared to experimental measurements from the newly calibrated Mu3e test setup.

## *Acknowledgements*

At this point I want to thank several people who made this thesis possible. First of all I want to thank Prof. Ulrich Straumann, Roman Gredig and Dr. Peter Robmann who made it possible to write this paper in the Mu3e-Group. A special thank goes to Roman Gredig who was always willing to support my work with his expertise in programming and experimental knowledge. But I also want to thank the people of the office I was allowed to work in, Nicolas Chiapolini, Christian Elsasser, Arno Gadola, Marco Tresch and Roman Gredig for thier support and the atmosphere, it has been a great time.

# Contents

<b>Abstract</b>	ii
<b>Acknowledgements</b>	iii
<b>1 Introduction</b>	1
<b>2 Mu3e Experiment</b>	2
2.1 Theoretical Background . . . . .	2
2.2 The Experiment . . . . .	3
2.3 The Detector . . . . .	3
2.4 The scintillating Fibres . . . . .	4
<b>3 Simulation</b>	6
3.1 Overview . . . . .	6
3.2 Estimations . . . . .	6
3.2.1 Energy deposition . . . . .	6
3.2.2 Photon yield . . . . .	8
3.3 Modifications to the Simulation tool-kit . . . . .	8
3.3.1 Geometry . . . . .	9
3.3.2 Materials . . . . .	10
3.3.3 Scintillating photons and surface-properties . . . . .	10
3.3.4 $^{90}\text{Sr}$ -Source . . . . .	12
3.4 Simulation Data . . . . .	15
3.4.1 General Analysis Overview . . . . .	15
3.4.2 $^{90}\text{Sr}$ -Source vs. Mono-energetic Source . . . . .	15
3.4.3 “Roughness” and Wrapping . . . . .	16
3.4.4 Second Scintillator . . . . .	17
<b>4 Experiment</b>	18
4.1 Experimental Setup . . . . .	18
4.2 Data Acquisition . . . . .	19
4.3 Experimental Data . . . . .	20
4.3.1 Analysis Overview . . . . .	20
4.3.2 Reproducibility of the measurement . . . . .	20
4.3.3 Optical coupling of the scintillator to the PMT . . . . .	22
4.3.4 Wrapping . . . . .	22

4.3.5	Second Scintillator . . . . .	23
<b>5</b>	<b>Results</b>	<b>24</b>
5.1	Reproducibility of the measurement . . . . .	24
5.2	Optical coupling . . . . .	24
5.3	Surface Properties . . . . .	25
5.4	Simulation vs. Reality . . . . .	25
5.5	Wrapping . . . . .	26
5.5.1	Simulation . . . . .	26
5.5.2	Experimental Results . . . . .	26
<b>6</b>	<b>Conclusion</b>	<b>27</b>
<b>Bibliography</b>		<b>28</b>

# Chapter 1

## Introduction

The standard model is currently the theoretical basis of particle physics. Several experiments are at the moment under development to search for physics beyond the well-established standard model. The proposed Mu3e-experiment is one of these experiments, searching for the lepton flavour violating decay  $\mu^+ \rightarrow e^+ e^- e^+$  with a proposed sensitivity of  $10^{-16}$ . Since the branching ratio is so small a high muon rate is needed to carry out the experiment. The  $\pi E5$  beam-line at Paul Scherer Institut (PSI) in Villingen Switzerland provides one of the worlds highest muon-rate and a new muon beam-line will be established within the next  $\sim 10$  years.

The Mu3e experiment is developed by groups of the University of Heidelberg, University of Geneva, PSI, ETH Zuerich and University of Zuerich. Due to very small branching ratio high spatial and timing resolution is needed for the detector. The proposed system contains a fibre tracking detector to establish a time resolution of  $< 1$  ns. A simulation of the fibres and the detector using GEANT4 [1] has been developed.

To gain confidence in the simulation experimental studies have been carried out in parallel. Using the physics of the simulation a well known scintillator was simulated and the data compared to the actual measurement using the newly calibrated Mu3e fibre test setup.

## Chapter 2

# Mu3e Experiment

### 2.1 Theoretical Background

The standard model conserves lepton flavour at tree levels. However various experiments such as SNO [2], SuperKamiokande [3], and KamLAND [4] have observed neutrino oscillations a direct proof of leptons flavour violation (LFV). The transitions  $\mu \rightarrow e$  and  $\tau \rightarrow \mu$  without neutrinos in the final state are possible if charged LFV (CLFV) is put in to consideration. By adding neutrino mixing in the standard model one can include CLFV, but due to the very small neutrino masses these processes are highly suppressed, with resulting branching ratios ( $10^{-50}$ ) way beyond any experimental sensitivity. An observation of CLFV would directly imply physics beyond the standard model. Therefore a new experiment at PSI has been proposed, pushing the upper limit for the decay  $\mu^+ \rightarrow e^+ e^- e^+$  to  $B < 10^{-16}$  [5].

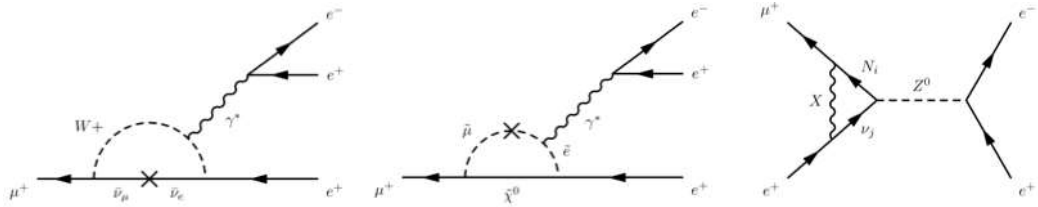


FIGURE 2.1: Possible  $\mu^+ \rightarrow e^+ e^- e^+$  mechanisms. From the left: neutrino mixing allowed within the standard model, a supersymmetric contribution, and a penguin diagram in the little Higgs model.

## 2.2 The Experiment

The momentum sum of the three decay particles of the  $\mu^+ \rightarrow e^+ e^- e^+$  decay has to vanish.

$$|\vec{p}_{tot}| = \left| \sum_i p_i \right| = 0 \text{ MeV/c} \quad (2.1)$$

And the total energy has to be the mass of the muon. Possible backgrounds are the internal conversion process  $\mu^+ \rightarrow e^+ e^- e^+ \nu_e \bar{\nu}_\mu$  and accidental coincident measurements of  $e^+ e^+ e^-$ . To suppress this random background, high time and vertex resolutions are needed ( $\leq 1 \text{ ns}$  and  $\leq 100 \mu\text{m}$ ). In order to reach the needed sensitivity a muon stopping rate of  $2 \cdot 10^9 \text{ s}^{-1}$  has to be achieved.

## 2.3 The Detector

Fig. 2.2 and Fig. 2.3. shows the proposed cylindrical detector which is positioned in a 1 T solenoidal magnetic field of 2.5 m length and 1 m diameter. The hollow aluminium double cone target is mounted in the centre of the detector and has a length of 10 cm and a diameter of 2 cm. The muon beam is aligned with the symmetry axis. The detector itself is divided in to five sub-detectors each with a length of 36 cm along the beam direction. The central section has an outer tracker made of three layers of scintillating plastic fibres with a diameter of 250  $\mu\text{m}$ . The scintillating fibres are mounted with an inner radius of 6 cm additionally two layers of silicon pixel detectors are placed at a radius of 7.6 cm and 8.9 cm. In addition the central section has an 12 cm long inner tracker with silicon pixels at 2.9 cm and 1.9 cm radius. The other subsections contain no inner tracking detector and instead of scintillating fibres use scintillator tiles.

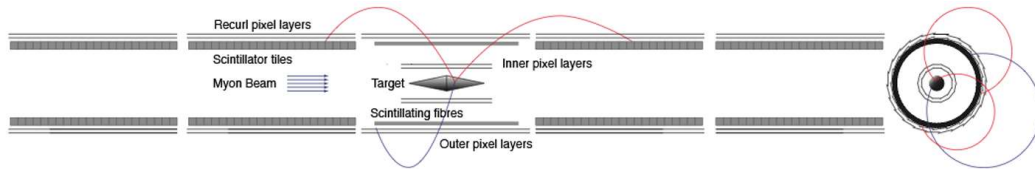


FIGURE 2.2: zr- and xy view of the proposed detector [5].

The concept is highly modular which allows for a staged approach:

- Phase 1a: In this stage only the Si layers of the central detector are installed handling a muon rate of  $2 \cdot 10^7 \text{ s}^{-1}$  provided by the  $\pi E5$  beam line at the PSI [6].

- Phase 1b: The central detector will be upgraded with the fibre detector and two recoil stations with their respective scintillating tile detectors. This additional timing resolution allows for the maximal muon rate of  $1 \cdot 10^8 \text{ s}^{-1}$  of the  $\pi E5$  beam line [6].
- Phase 2: All five sub-detectors are in place. This is the final stage of the detector development and the new proposed beam-line (HiMB) will provide the needed  $2 \cdot 10^9 \text{ s}^{-1}$  muons for the expected final sensitivity.

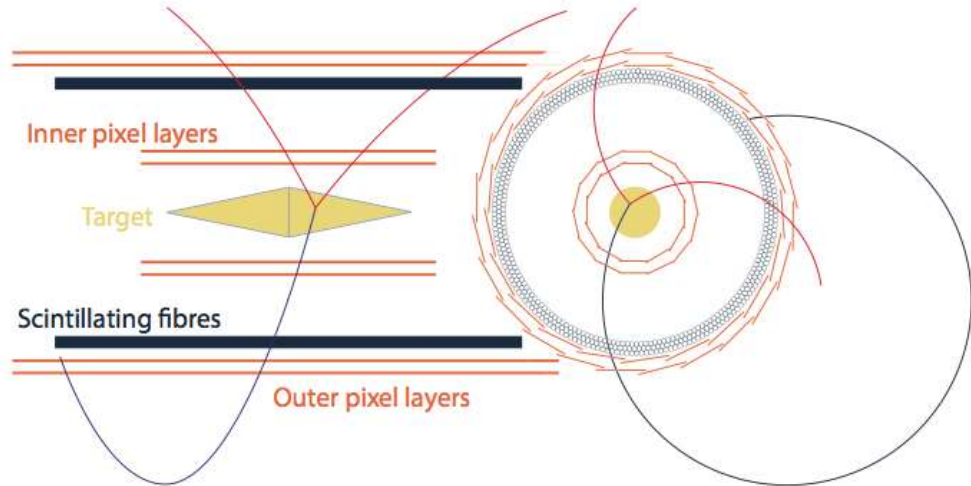


FIGURE 2.3: Close up view of the proposed central module of Mu3e-detector, scintillating fibres highlighted in blue [5].

## 2.4 The scintillating Fibres

In collaboration with the University of Geneva and ETH the Mu3e group at UZH develops the scintillating fibre tracker. The readout of the fibres will be done by silicon photomultipliers. The small size and the possibility to operate them in high magnetic fields makes them ideal for the experiment. To study the optical response of the fibres a simulation tool-kit has been developed using Geant4. To minimise the required computation time the simulation has two sequential modes of operation.

- A standalone simulation of the fibres allows for in-dept analysis of the geometry, the generation, propagation and absorption of the photons can be directly related and parameterized to the deposited energy, crossing position and surface effects.
- A simulation of the whole detector, which no longer tracks the scintillation light but uses the parameterized fibre response instead.

The simulation of the fibres and the light propagation allows comparing of different configurations of the fibre geometry and coating. Spatial distribution of the photons

and their time distribution have been studied. Typically 12 photons will reach one end of the fibre where they will be detected with a SiPM array with an efficiency of typically 50%. The simulations indicate a combined time resolution of the fibres and the SiPM [7] of around 400 ps [8].

# Chapter 3

## Simulation

### 3.1 Overview

To verify the simulation tool-kit data for the fibre tracker we modified the simulation by changing the geometry of the scintillator and the scintillating material to match the experiment we preformed. Since we are dealing with optical processes surface properties have a big impact on the resulting optical photon pick up by the detectors on either end of the scintillator. To get a handle on this studies of the photon yield due to different surface properties were carried out. We simulated data for different surface roughnesses and different commonly used wrapping materials. To simulate the electrons used in the experiment a  $^{90}\text{Sr}$ -Source was programmed.

### 3.2 Estimations

#### 3.2.1 Energy deposition

To get a feeling for the simulated and measured data a rough estimation about the energy deposition was done.

The mean energy loss during an interaction between a charged particle and a material or the stopping power is described by the Bethe-Bloch formula [9]:

$$\frac{-dE}{dX} = K z^2 \frac{Z}{A} \frac{1}{\beta^2} \left[ \frac{1}{2} \ln \frac{2m_e c^2 \beta^2 \gamma^2 T_{max}}{I^2} - \beta^2 - \frac{\delta}{2} - \frac{C}{Z} \right] \quad (3.1)$$

with

$$K = \frac{4\pi e^4}{c^2 m_e} N_A = 0.31 \text{ MeV cm}^{-2} \text{ g}^{-1} \quad (3.2)$$

$$T_{max} = \frac{2m_e c^2 \beta^2 \gamma^2}{1 + 2\gamma m_e/M + (m_e/M)^2} \quad (3.3)$$

$I$ : mean excitation energy

$Z$ : atomic number

$A$ : mass number of absorber

$z$ : Charge of particle

$M$ : Mass of the particle

$\delta(\beta)$ : density correction due to polarisation, important for high energies

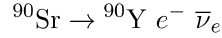
$C/Z$ : correction close to shell boundaries, relevant for small energies

This formula nevertheless describing the energy loss of a charged particle in an interaction with a material is not true for the interaction between electrons and matter. The Bethe-Bloch formula has to be modified to hold true for such interactions. The exact calculation of electron-electron scattering plus shielding gives the following formula [10]:

$$\frac{-dE}{dX} = K \frac{Z}{A} \frac{1}{\beta^2} \left[ \frac{m_e c^2 \gamma \beta^2 \sqrt{\gamma - 1}}{\sqrt{2I}} + \frac{1}{2}(1 - \beta^2) - \frac{2\gamma - 1}{2\gamma^2} \ln 2 + \frac{1}{16} \left( \frac{\gamma - 1}{\gamma} \right)^2 - \frac{\delta}{2} \right] \quad (3.4)$$

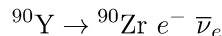
The scintillation material (BC-412) is composed of  $C_{10}H_{11}$  as an approximation for  $Z$ ,  $A$  and  $I$ . We took the average value for the composite which gave us a value of  $Z = \frac{71}{21} \cong 3.4$ ,  $A = \frac{131}{21} \cong 6.24$  and  $I = 12.17 \text{ eV}$  [11].

In the experimental setup we use a  $^{90}\text{Sr}$ -Source.  $^{90}\text{Sr}$  has a half-life time of 28.79 years and undergoes a  $\beta^-$ -decay:



with a Q-value of 0.546 MeV [12].

$^{90}\text{Y}$  with a half-life time of 64.05 h it self also undergoes a  $\beta^-$ -decay:



and a Q-value of 2.28 MeV [12].

The Q-value is distributed to the electron and the antineutrino resulting in a  $\beta$ -continuum. Since these are just rough approximations to get a feeling for the plausibility of the simulation and the experiment the energy of the electron was set to be the Q-value for the calculations.

Using these assumptions with equation (3.4) gives  $-\frac{dE}{dX} \cong 9.6 \text{ MeV cm}^2 \text{ g}^{-1}$  for the electron of the  ${}^{90}\text{Sr } \beta^-$ -decay and  $-\frac{dE}{dX} \cong 2.2 \text{ MeV cm}^2 \text{ g}^{-1}$  for the one of the  ${}^{90}\text{Y } \beta^-$ -decay.

### 3.2.2 Photon yield

In order to validate the photon readout of the simulation a quick back of the envelope calculation was done first. In section 3.2.1 an approximation for the energy deposition was done which gives us roughly  $0.25 \text{ MeV cm}^{-1}$  of stopping power for our scintillator and the  ${}^{90}\text{Y}$ . With our setup  $0.5 \text{ MeV}$  will be deposited in the material. The scintillation-yield of BC-412 is 11 400 photons/MeV resulting in a light-output of 5700 photons /electron [11]. Assuming the photons are all generated in a single point and isotropic distributed over space we can calculate how many photons we can expect to detect with out a single reflexion. To do this we compare the area of the scintillator square up against the detector and the  $4\pi$ -solid-angle, which results in a  $\sim 17$  photons detected on each end of the scintillator. In the calculation the quantum efficiency of the PMT's was neglected.

Now lets take into account all the photons which are at least reflected once inside the scintillator. The scintillator has a refraction index  $n$  of 1.42 the air surrounding it has  $\sim 1$  resulting in a critical angle of  $45^\circ$  photons emitted under a larger angle will leave the scintillator. The scintillator is 100 mm long. With this information and the critical angle we can again calculate the basearea of the cone and compare it with the whole  $4\pi$ -solid-angle. If we consider all photons which are emitted with an angle of  $\leq 45^\circ$  the detected output increases to 1500 photons per detector still neglecting the quantum efficiency of the photomultiplier tubes (PMT).

## 3.3 Modifications to the Simulation tool-kit

In order to check the simulation on physical coherence with real data we changed the existing tool-kit for the fibres to match the experimental setup (see Fig.4.1).

### 3.3.1 Geometry

The first scintillator was a cuboid  $100\text{ mm} \times 20\text{ mm} \times 6.25\text{ mm}$ . The estimations in section 3.2.1 showed that most of the electrons emitted by the source can not traverse the whole of the scintillator, most of them are absorbed in the material. This results in a low trigger rate. To increase the rate of triggering events the scintillator was milled down to 2 mm in the center. This resulted in a 10 mm wide and 4.75 mm deep notch in the center of the scintillator see Fig.3.1. This modified scintillator was implemented in the simulation. As in the experiment so called optical interface pads [13] were added in between the detector tubes and the scintillator.



---

FIGURE 3.1: The first used scintillator  $100\text{ mm} \times 20\text{ mm} \times 6.25\text{ mm}$  with the 4.75 mm deep notch in the center.

In a later stage of the work a second scintillator cuboid  $100\text{ mm} \times 20\text{ mm} \times 2\text{ mm}$  was implemented to get a cross check on the data. A third detector was implemented to be used as a trigger. This trigger was placed opposite the particle source. The complete geometry of the simulation for the first scintillator can be seen in Fig.3.2.

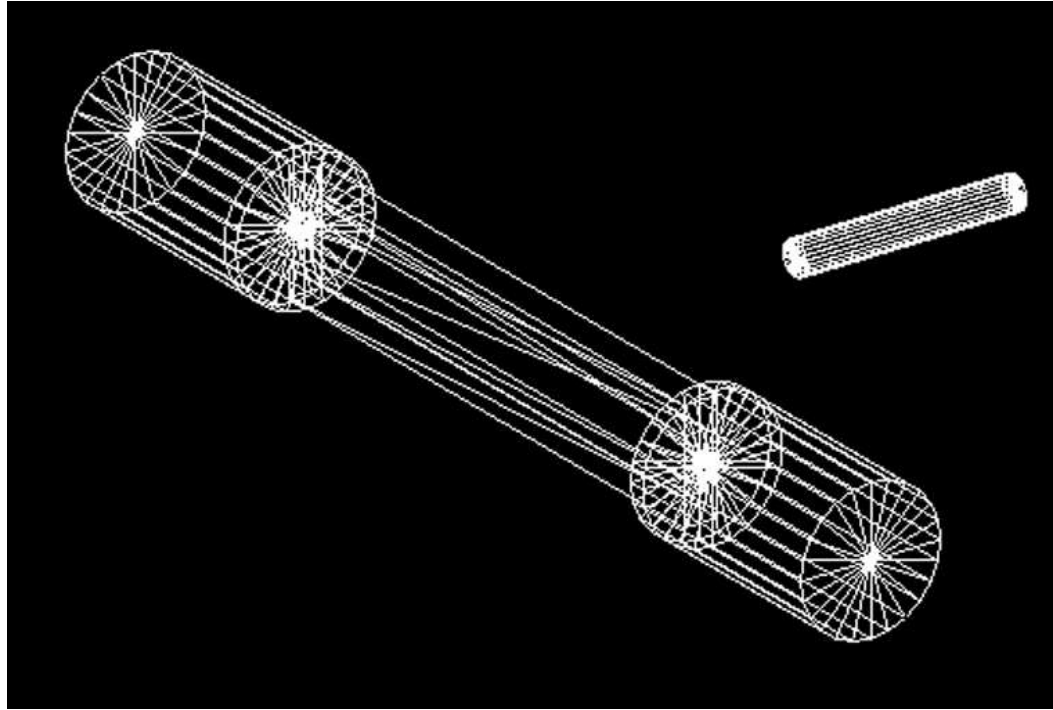


FIGURE 3.2: A screenshot of the simulation geometry. The scintillator is situated in the center on both ends are the photon-detectors with optical interface pads and on right is the small detector which was used as a trigger.

### 3.3.2 Materials

Geant4 offers a large database of materials. For the modification of the existing simulation we added or changed existing properties of materials. For example the density, light attenuation, scintillating properties, refraction coefficients had to be modified or added to the already existing materials. As an example in Fig.3.3 the photon output of the used scintillation material (BC-412) [11] is shown which we implemented in the material-database.

### 3.3.3 Scintillating photons and surface-properties

Since we want to detect 10 to 1500 photons per event (see estimation in section 3.2.2) optical properties of the scintillator, optical interface pads, and the photomultiplier-tubes are important. Scintillating photons can be simulated in Geant4 [1]. They can be transmitted, absorbed and reflected. To simulate the experimental situation as complete as possible the optical properties of the used parts were implemented.

Boundary processes play an important part in the overall photon yield at the detectors. To simulate boundary processes Geant provides different models. This models allowed

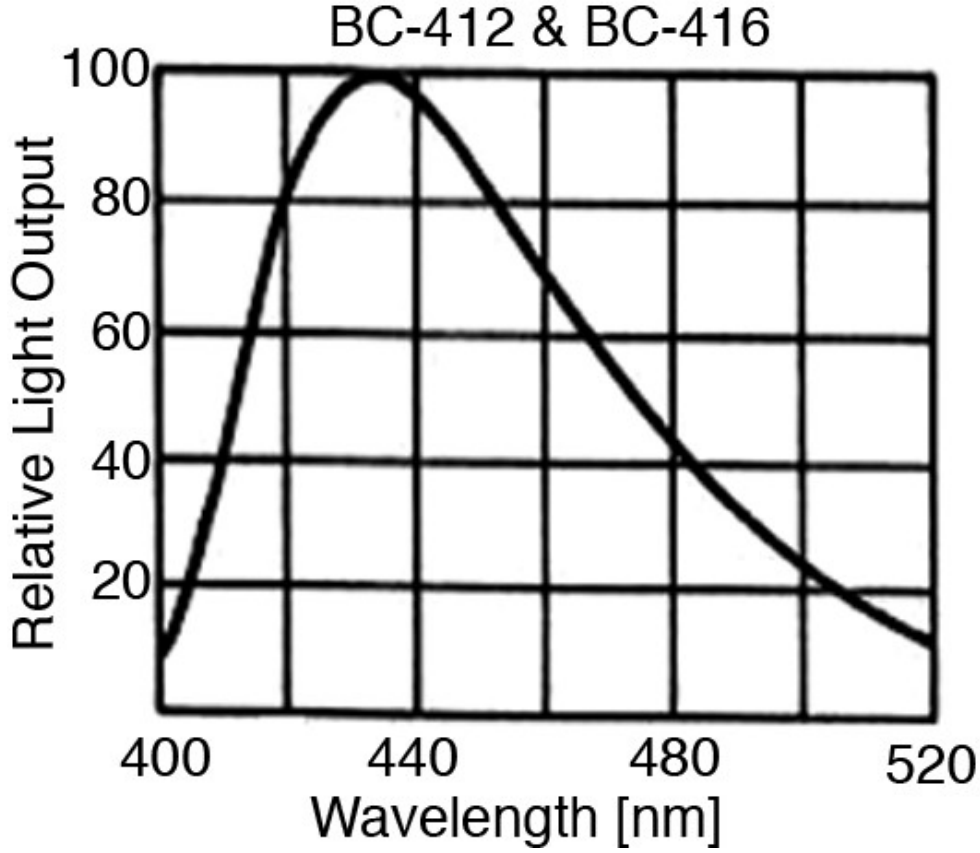


FIGURE 3.3: Emission Spectra of the scintillating material BC-412 [11].

us to simulate boundary processes for optical photons. The general characteristics of the surface can be modeled i.e. the transition between an dielectric-dielectric or dielectric-metal, refraction-coefficients and the roughness of the surface. General properties of the process are given by the defined dielectric-dielectric, dielectric-metal transitions. The roughness describing how polished a surface is, is simulated by micro-facets every time an optical photon crosses the surface a random angle is assigned to the micro-facet. The standard-deviation of the distribution of this angle  $\alpha$  can be set to match the properties of the processed surface. In the rest of this thesis we will refer to this as  $\sigma$ -alpha. In Table 3.1 different  $\sigma$ -alpha of processed surfaces are given.

TABLE 3.1:  $\sigma$ -alpha of different processed surfaces (in degree and radian) [14].

Polished	Etched	Ground
$1.3^\circ$	$3.8^\circ$	$12^\circ$
0.0227	0.0663	0.2094

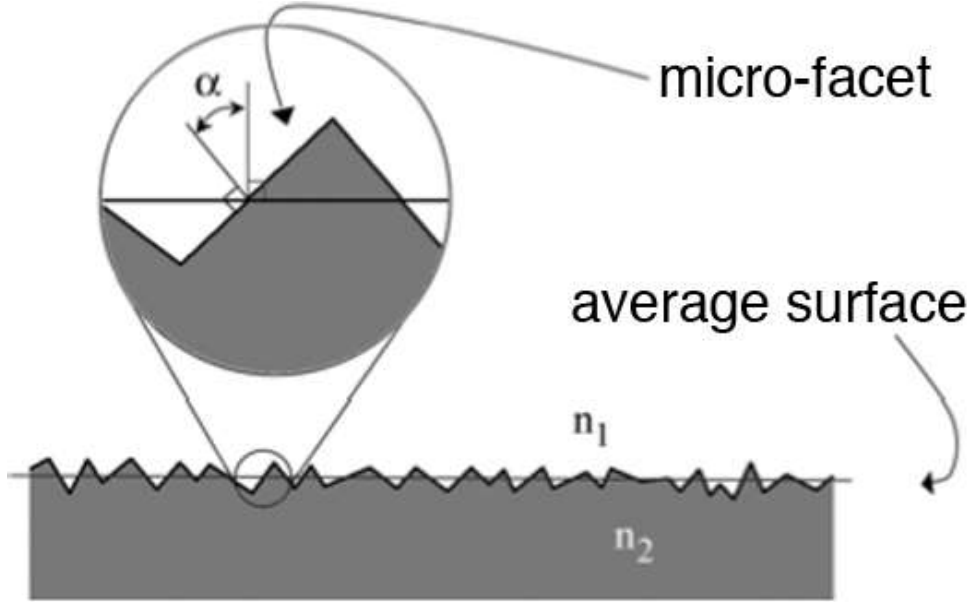


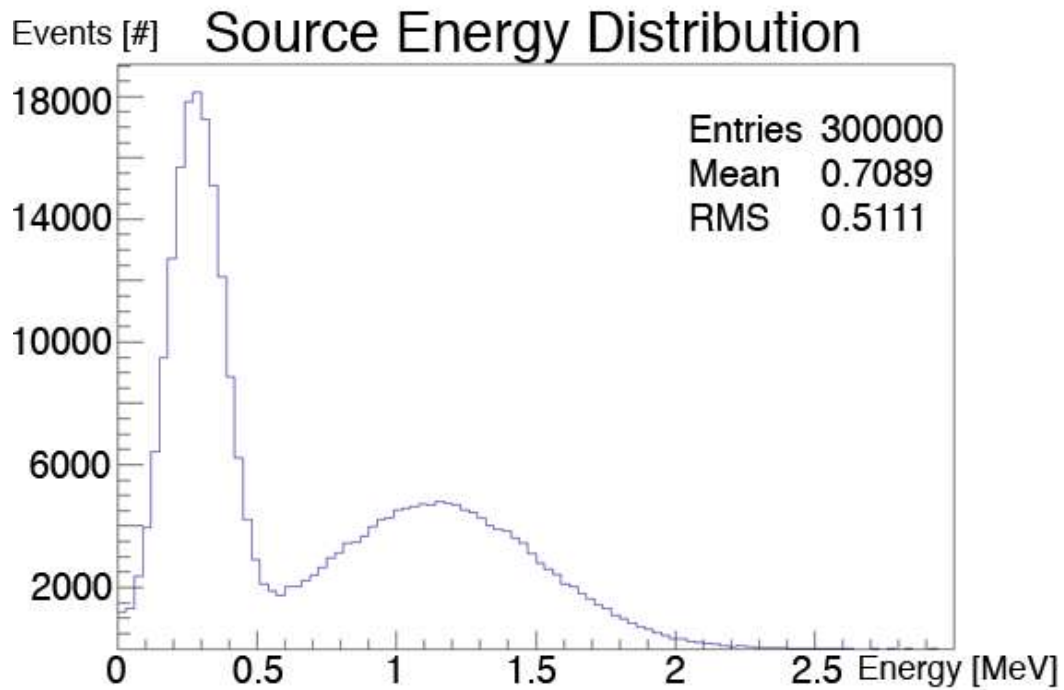
FIGURE 3.4: The angle  $\alpha$  is the angle between the surface normal and the normal of the micro-facet.  $\sigma$ -alpha describes the standard-deviation of gaussian distribution of the angle  $\alpha$  [14].

### 3.3.4 $^{90}\text{Sr}$ -Source

Geant4 offers with the particle source class [15] an easy way to program a wide variety of sources. Allowing programming momentum-, angle-, energy distribution the G4GeneralParticleSource class was used to model the  $^{90}\text{Sr}$ -Source used in the experimental setup. To optimize time management an approximation was made using two Gaussian distributions at the mean energy with  $3\sigma$  of all particles emitted in the energy range of the  $^{90}\text{Sr}$  and  $^{90}\text{Y}$  betadecay channel (see section 3.2.1). The resulting energy distribution is plotted in Fig.3.5 An angular distribution of the emitted electrons to the Lamberts cosine-law was programmed see Fig.3.6 and the dimensions of the source were implemented. Since the half-life time of  $^{90}\text{Y}$  is short compared to the one of  $^{90}\text{Sr}$  the assumption was made that the emitted electrons are equally distributed between the two decay channels.

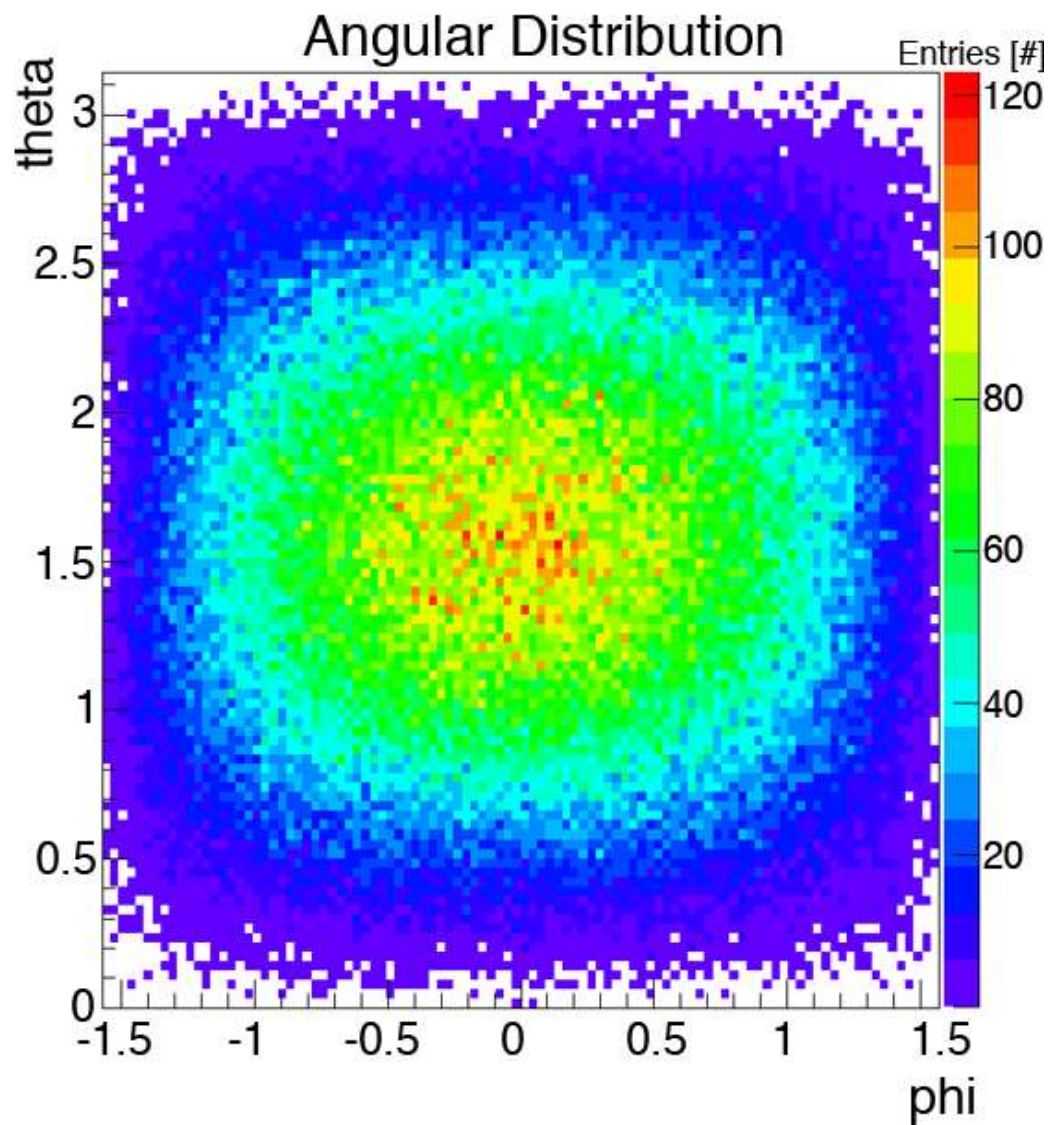
As the estimations in section 3.2.1 showed most of the emitted electrons of the  $^{90}\text{Sr}$ -Source won't even traverse the whole scintillator and trigger the data-acquisition. Due to the angular and energy-distributions the numbers of actual triggering events in the simulations was less than 1/700 per emitted particle (Table 3.2). In order to minimize the used computation time the  $^{90}\text{Sr}$ -Source was approximated with a simple mono-energetic source set to 2.28 MeV without an angular distribution. To verify this assumption one

longtime simulation was done using the above described  ${}^{90}\text{Sr}$ -Source and the data was compared (see section 3.4.2).



---

FIGURE 3.5: Energy distribution of the approximated  ${}^{90}\text{Sr}$ -Source.



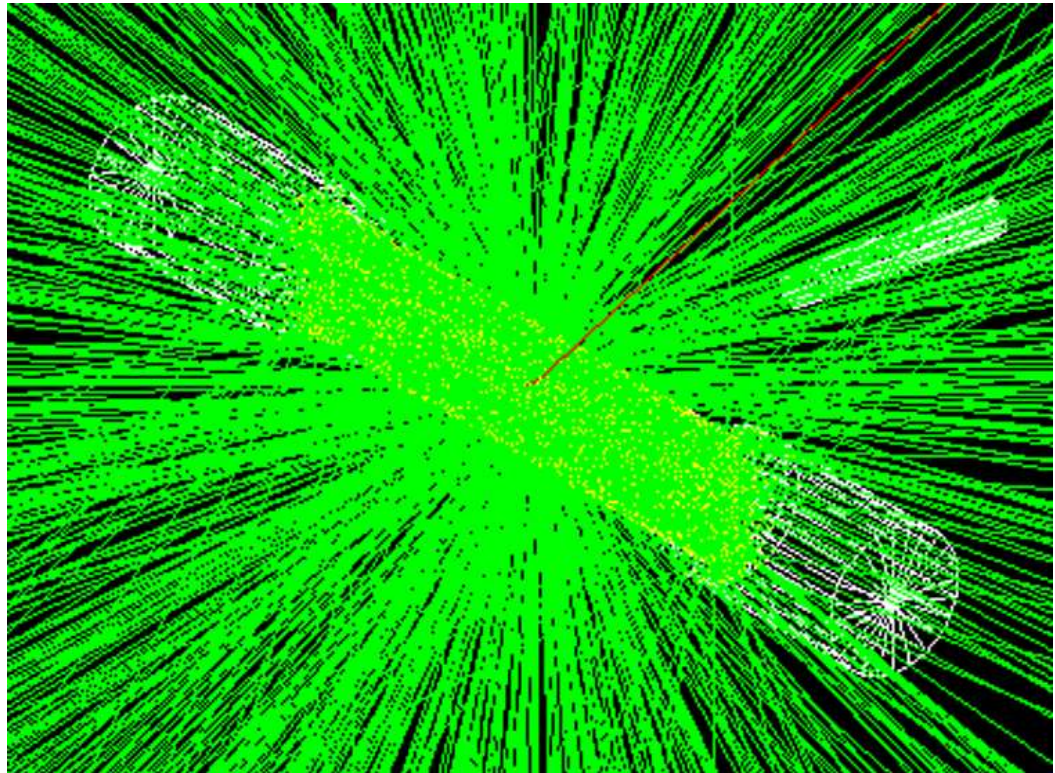
---

FIGURE 3.6: Angular distribution of the approximated  $^{90}\text{Sr}$ -Source.

## 3.4 Simulation Data

### 3.4.1 General Analysis Overview

The analysis of the simulated data was done in ROOT [16]. The data of the simulation tool-kit was converted into ROOT-files. With RooFit [17] a convolution of a landau-and gaussian-distribution was fitted on the data. In the tables the most likely value of the landau-distribution of the fit is given. An assumed quantum efficiency of the photomultiplier tubes of 0.32 was taken in to account in the analysis [18]. Fig. 3.7 shows the simulation of one event in green are the scintillation photons and in red the electron from the source.




---

FIGURE 3.7: One simulated event in green scintillation photons and in red the electron from the source.

### 3.4.2 $^{90}\text{Sr}$ -Source vs. Mono-energetic Source

To validate the assumption in section 3.3.4 a simulation run of 300 000 events with the first geometry and a  $\sigma$ -alpha of 0.01 was made consuming over a week of computation time on a single machine. The data in Table 3.2 shows that in order to reach a similar

number of triggering events compared with the mono-energetic particle source in Table 3.3 a total number of 300 000 events had to be simulated and the corresponding data stored. Although a  $\sim 25\%$  higher light yield was achieved (compare Table 3.3  $\sigma$ -alpha 0.01), it doesn't justify the time needed to do a single simulation and our assumption to use a mono-energetic source seems legitimate.

TABLE 3.2: Simulated Data, for the first used scintillator geometry using the  $^{90}\text{Sr}$ -Source

# triggering Events	Right PMT [ $\gamma/\text{Event}$ ]	Left PMT [ $\gamma/\text{Event}$ ]
404	$308.98 \pm 0.01$	$310.54 \pm 0.14$

### 3.4.3 "Roughness" and Wrapping

We ran multiple simulations to check the influence of different  $\sigma$ -alpha (see section 3.3.3) and wrapping materials. In Table 3.3 the resulting photon output is listed which corresponds with the data in Fig.3.8.

TABLE 3.3: Simulated Data, dependency of the light output due to the "roughness"

$\sigma$ -alpha	# of triggering Events	Right PMT [ $\gamma/\text{Event}$ ]	Left PMT [ $\gamma/\text{Event}$ ]
perfect	565	$244.3 \pm 1.5$	$243.9 \pm 1.5$
0.00	540	$241.6 \pm 1.3$	$242.8 \pm 1.5$
0.01	514	$243.8 \pm 1.5$	$243.5 \pm 1.5$
0.0125	520	$243.0 \pm 1.5$	$242.7 \pm 1.6$
0.015	474	$237.8 \pm 1.5$	$239.3 \pm 1.5$
0.0175	521	$240.5 \pm 1.6$	$240.8 \pm 1.5$
0.02	519	$238.8 \pm 1.4$	$236.8 \pm 1.4$
0.05	537	$209.9 \pm 1.3$	$210.2 \pm 1.3$
0.07	517	$200.7 \pm 1.3$	$200.9 \pm 1.2$
0.1	494	$184.4 \pm 1.2$	$184.4 \pm 1.2$
0.15	505	$168.6 \pm 1.1$	$167.9 \pm 1.1$
0.2	517	$151.4 \pm 1.2$	$152.3 \pm 1.1$

In experimental setups scintillators are often wrapped to maximize the photon output and to shield them from outside light [19]. We simulated the two most commonly used materials for wrapping scintillators. The simulated photon output of the so wrapped scintillator with a  $\sigma$ -alpha of 0.01 is listed in Table 3.4.

TABLE 3.4: Simulated Data, different commonly used wrapping materials

wrapping	# of triggering Events	Right PMT [ $\gamma/\text{Event}$ ]	Left PMT [ $\gamma/\text{Event}$ ]
aluminium	529	$275.6 \pm 1.6$	$275.9 \pm 1.6$
teflon	515	$470.8 \pm 2.5$	$471.0 \pm 2.5$

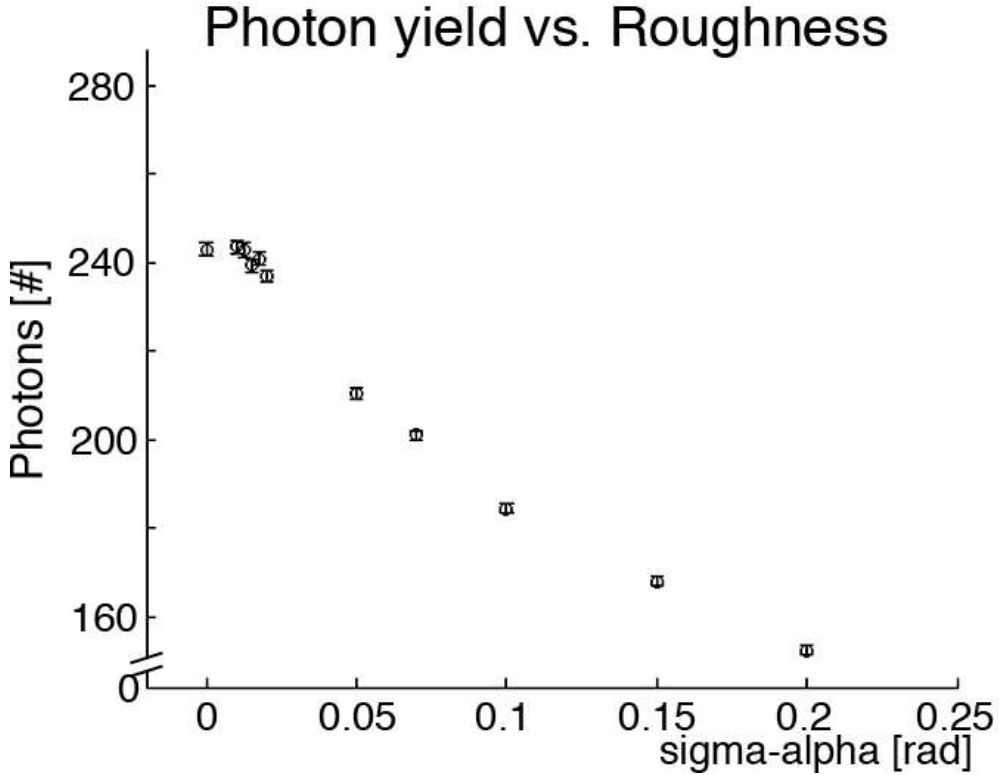


FIGURE 3.8: Dependency of photon pick up due to different  $\sigma$ -alpha. (For the left PMT)

### 3.4.4 Second Scintillator

Polishing the notch of the first scintillator was problematic and the surface was covered with hairline cracks. To cross check the results of the measurement with the first scintillator (Fig. 3.1) a second scintillator was processed. In order to get rid of the notch the second scintillator was milled down completely to 2 mm. To compare the measurements with this second scintillator the simulation was modified for the second scintillator. The simulation was run for a  $\sigma$ -alpha of 0.01 and a naked scintillator and one wrapped with teflon tape. In Table 3.5 the results of the simulation are listed.

TABLE 3.5: Simulated Data, for the second used scintillator geometry

wrapping	# of triggering Events	Right PMT [ $\gamma$ /Event]	Left PMT [ $\gamma$ /Event]
none	1174	$114.94 \pm 0.53$	$115.55 \pm 0.61$
teflon	1247	$211.64 \pm 0.92$	$211.90 \pm 0.94$

# Chapter 4

# Experiment

## 4.1 Experimental Setup

To check the quality of the simulation different measurements were done using the test setup in Fig.4.1 and 4.2. The scintillator is in the center of the setup mounted between the two PMT's (PMT2 and 3). For the dimensions of the scintillator see section 3.3.1. The PMTs are protected with a copper housing. To ensure a good optical coupling of the scintillator on the PMT self-wetting optical interface pads (OIP) were used. With the tension of rubber-bands the PMTs are pushed on the scintillator holding it in place. The black PMT (PMT1) is used as the trigger. Opposite this trigger the  $^{90}\text{Sr}$ -Source is placed. The calibration of the PMTs was done earlier.

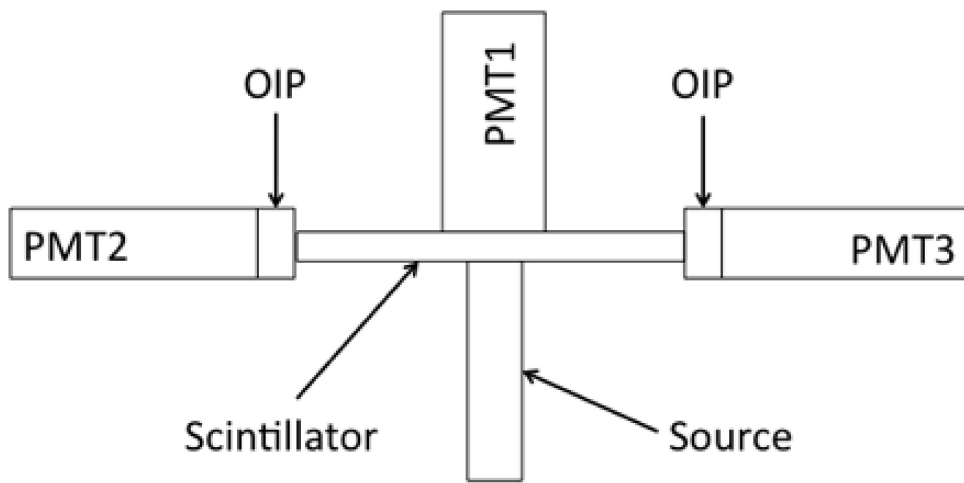


FIGURE 4.1: The schematic experimental setup.

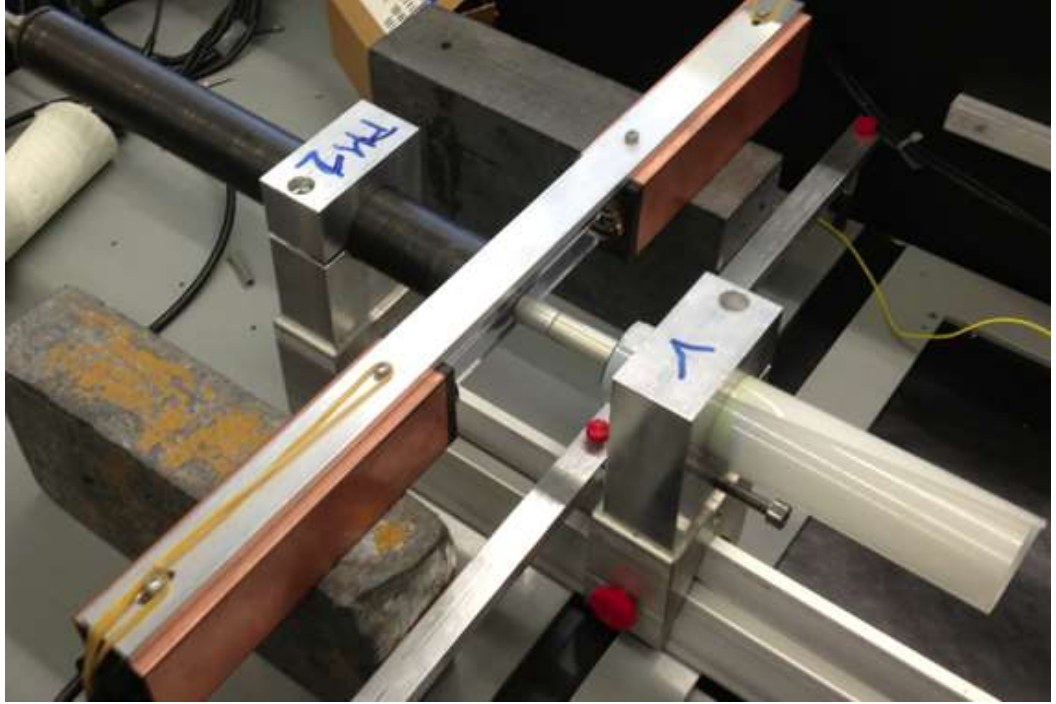


FIGURE 4.2: The real experimental setup. In this case without the optical interface pads in place.

## 4.2 Data Acquisition

In this section we take a look at the read out electronics of the experiment (see Fig.4.3). The signal from the PMT on either side of the scintillator (PMT 2 and 3) is processed by a fanout, an attenuator (ATT) and a delayed to match the gate signal on the ADC. The triggering signal of the trigger PMT (PMT 1) is first processed by a fanout. The analog signal of the trigger is then digitalized by a discriminator (DISC). The triggering signal gets coincidenced with a signal of a D-trigger. The D-trigger allows for a cross check with the dead time of the computer acquiring the data. If the computer is ready and a triggering signal is picked up the gate is opened on the ADC. The look-at-me (LAM) starts the data acquisition of the computer. During the data acquisition the D-trigger denies the processing of additional triggering signals. After the read out the computer readies the system again via the D-trigger.

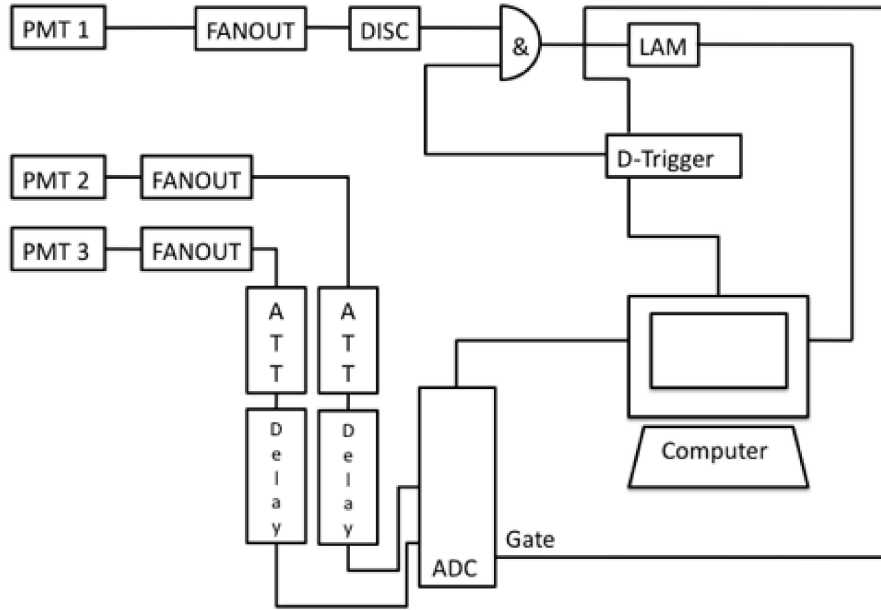


FIGURE 4.3: The readout electronics.

## 4.3 Experimental Data

### 4.3.1 Analysis Overview

All experimental measurements were done over a total number 100 000 triggering events. As in the analysis of the simulated data with RooFit a convolution of a landau- and a gaussian was fitted on the acquired data. To compute the error on the most likely photon output the errors on the fit, the pedestal and the calibration of the PMT's were propagated.

### 4.3.2 Reproducibility of the measurement

One of the aspects of the experiment which had to be verified is the reproducibility of the measurement. To check this the scintillator was five times remounted in the experiment and consecutive measurements were done with and without optical interface pads (OIP). The resulting data is listed in Table 4.1 and 4.2.

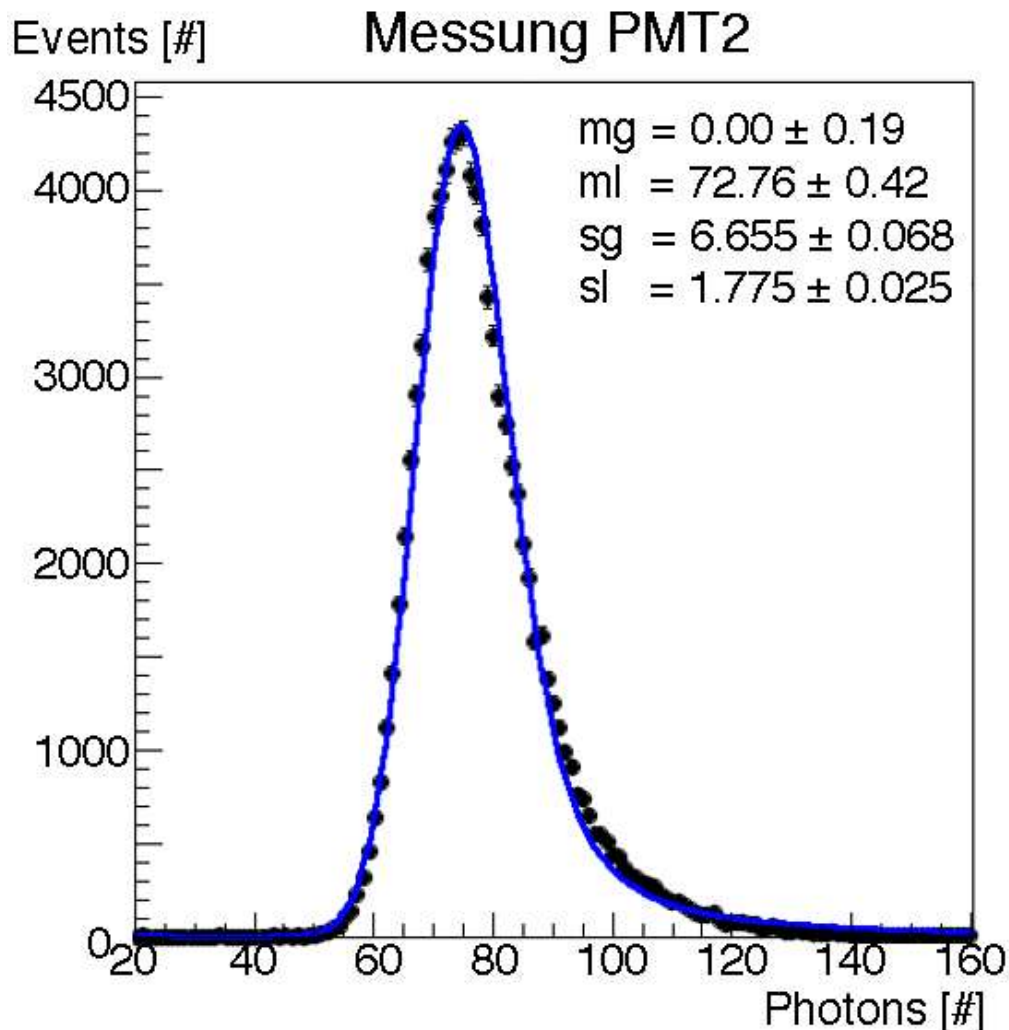


FIGURE 4.4: Example for the fit of the convolution of a landau- and gaussian on the data.

TABLE 4.1: Experimental Data, scintillator coupled with OIP to the PMT and the resulting mean photon yield.

Right PMT [ $\gamma$ /Event]	Left PMT [ $\gamma$ /Event]
$81.45 \pm 6.84$	$83.88 \pm 7.26$
$83.91 \pm 6.95$	$83.43 \pm 7.28$
$81.69 \pm 6.80$	$78.75 \pm 7.27$
$84.11 \pm 6.97$	$79.45 \pm 7.24$
$83.58 \pm 7.01$	$77.67 \pm 7.14$
$82.95 \pm 0.25$	$80.63 \pm 0.57$

### 4.3.3 Optical coupling of the scintillator to the PMT

An ever recurring question is the coupling of optical parts. In order to check for the advantages of optical interface pads five measurements without them were preformed. As stated in section 4.3.2 the scintillator was remounted between every measurement. The measured data is listed in Table 4.2.

TABLE 4.2: Experimental Data, scintillator coupled without OIP to the PMT and the resulting mean photon yield.

Right PMT [ $\gamma$ /Event]	Left PMT [ $\gamma$ /Event]
$71.71 \pm 6.93$	$74.07 \pm 7.14$
$71.31 \pm 6.82$	$73.70 \pm 7.19$
$69.25 \pm 6.85$	$73.68 \pm 7.17$
$69.14 \pm 6.85$	$74.78 \pm 7.21$
$70.81 \pm 6.88$	$72.51 \pm 7.21$
$70.44 \pm 0.24$	$73.75 \pm 0.17$

### 4.3.4 Wrapping

As stated in section 3.4.3 scintillators are often wrapped. Two commonly used materials are teflon and aluminium. To compare the simulated data multiple measurements with the aluminium and teflon wrapped scintillators were carried out. The results are listed in Table 4.3 and 4.4. The result for the second scintillator wrapped with teflon is listed in Table 4.6.

TABLE 4.3: Experimental Data, scintillator wrapped in aluminium foil (dull) coupled with OIP to the PMT's and the resulting mean photon yield.

Right PMT [ $\gamma$ /Event]	Left PMT [ $\gamma$ /Event]
$88.82 \pm 6.94$	$83.95 \pm 7.45$
$86.76 \pm 6.98$	$84.48 \pm 7.33$
$82.75 \pm 7.16$	$88.62 \pm 7.50$
$88.70 \pm 6.97$	$85.97 \pm 7.31$
$88.83 \pm 7.02$	$81.36 \pm 7.41$
$87.17 \pm 0.52$	$84.88 \pm 0.53$

TABLE 4.4: Experimental Data, scintillator wrapped in aluminium foil (shiny) coupled with OIP to the PMT's and the resulting mean photon yield.

Right PMT [ $\gamma/\text{Event}$ ]	Left PMT [ $\gamma/\text{Event}$ ]
$87.98 \pm 7.00$	$81.35 \pm 7.30$
$86.34 \pm 7.07$	$82.69 \pm 7.28$
$84.65 \pm 7.10$	$82.59 \pm 7.16$
$81.69 \pm 6.78$	$85.44 \pm 7.10$
$87.68 \pm 7.01$	$80.91 \pm 7.06$
$85.67 \pm 0.52$	$82.60 \pm 0.35$

TABLE 4.5: Experimental Data, scintillator wrapped in teflon tape coupled with OIP to the PMT's and the resulting mean photon yield.

Right PMT [ $\gamma/\text{Event}$ ]	Left PMT [ $\gamma/\text{Event}$ ]
$83.30 \pm 6.85$	$84.43 \pm 7.47$
$87.60 \pm 6.79$	$86.44 \pm 7.46$
$84.62 \pm 6.96$	$85.94 \pm 7.74$
$84.61 \pm 7.01$	$86.11 \pm 7.78$
$83.32 \pm 7.14$	$81.95 \pm 7.48$
$84.79 \pm 0.33$	$84.97 \pm 0.37$

### 4.3.5 Second Scintillator

The results of the measurements for the second scintillator are listed in Tabel4.6.

TABLE 4.6: Experimental Data, for the second used scintillator geometry coupled with OIP to the PMT's

wrapping	Right PMT [ $\gamma/\text{Event}$ ]	Left PMT [ $\gamma/\text{Event}$ ]
none	$86.60 \pm 7.13$	$90.83 \pm 7.95$
teflon	$102.36 \pm 7.48$	$96.12 \pm 7.91$

# Chapter 5

## Results

### 5.1 Reproducibility of the measurement

As stated in section 4.3.2 one of the questions which had to be answered first was how reproducible the experiment is. The mean of the data in Table 4.1 and 4.2 was calculated for each side separately and the single measurements were compared to the mean. This indicates on average deviations of 1.33(8) % and 2.99(21) % from the mean with OIP for the right and left side respectively and 1.42(11) % and 0.74(15) % without OIP. The calculation show a maximal deviation of 4.02 % for the first measurement with OIP on the left side.

The results show better reproducibility for the experiment without optical interface pads. This could be due to the instability of the scintillator mounting resulting in a more cautious handling of inserting the scintillator in the experimental setup. A possibility for the fact that the photon yield of the left PMT with OIP was less stable could be the accumulation of dust and dirt on the OIP for example from the fabric gloves which were worn to handle the scintillator. But overall the results indicate a good reproducibility and for further measurements the scintillator was not moved between two consecutive experiments.

### 5.2 Optical coupling

Coupling of optical parts is crucial in experiments whit small numbers of photons. To enable a good transition of photons between parts the refraction indices  $n$  should be as equal as possible. Optical interface pads fulfill this requirement and let the parts fit tight and nicely together.

Comparing the mean photon pick up of the setup with and without OIP shows a increased photon pick up for the OIP Setup of 13.5(29) %. This is the mean increase for both PMTs. Since the photon yield of the left PMT was decreasing during the measurements (see Table 4.1 and section 5.1) further measurements would be necessary to get a better result in this respect.

### 5.3 Surface Properties

The results of the simulation for different  $\sigma$ -alpha (see Table 3.3 and Fig. 3.8) show that especially with low numbers of photons the reduced photon output due to the loss from boundary processes is not negligible. The data indicates a photon loss of 2.30(2) % to 21.73(19) % for typically processed surfaces ( $\sigma$ -alpha 0.02 (polished) and 0.07 (etched) compare Table 3.1). Understanding and including surface properties into a simulation is crucial for a good result.

### 5.4 Simulation vs. Reality

In general we simulated more photons than were measured actually. Comparing the mean of Table 4.1 and the results of the simulation in Table 3.3 shows that the number of simulated photons is between a factor of 1.836(16) to 2.945(20) for a  $\sigma$ -alpha of 0.2 and a perfect surface higher then the measured value.

The first impressions let us believe that this discrepancy could be due to age of the scintillator and the stress it was subject of during processing. In Figure 3.1 one can see the hairline cracks in the upper right of the scintillator. Secondly the geometry in it self might hold less efficient properties for guiding the scintillation light to the PMT's. Other flaws may concern the simulation for example was the scintillation light yield of the used scintillation material given as the percentage of the light output of anthracene or the optical properties of the pads which were incomplete.

The optical appearance of the second scintillator was better. There were less hairline cracks on the surface and the geometry is less complex compared with the first scintillator. Comparing the simulated data in Table 3.5 and the measurements in Table 4.6 show a mismatch of a factor 1.272(112) which indicates a good agreement of the simulation and the real experiment. Comparing the Table 3.5 and 3.3 ( $\sigma$ -alpha 0.01) show a different light output for both scintillator although in both cases the same thickness of scintillation material was in the path of the incoming electron. This might indicate problems with the simulation and/or the first geometry which is not yet completely understood

and further simulations and measurements might be necessary to fully understand the influence of the geometry on the photon yield.

## 5.5 Wrapping

### 5.5.1 Simulation

The simulated data in Table 3.3 and 3.4 show a 13.04(11) % increased photon output in the simulation for the aluminium wrapped and 93.11(70) % for the teflon wrapped scintillator. The first result is in good agreement with the results of different other experiments. The results for teflon seams unrealistic compare with the results in section 5.5.2 and further investigations in the simulation have to be carried out to understand this discrepancy.

### 5.5.2 Experimental Results

Wrapping our scintillator was difficult. Especially in the notch it was hard to get a good contact between the wrapping material and the scintillation material. The results in Table 4.3 and 4.4 indicate a comparable increased photon output for both sides of the aluminium-foil. Wrapping the scintillator in aluminium-foil resulted in a up to 5.08(3) % increased photon yield. The results in Table 4.5 are less promising. With the teflon the light output increased just by 2.43(1) %. This might suggest that wrapping scintillators in teflon is inferior to aluminium but it was especially hard to wrap our scintillator with teflon-tape. In addition the influence of the wrapping on the light guiding properties of the first geometry is not understood and might be an interesting topic for further measurements and simulations. The results for the second scintillator in Table 4.6 confirms that a teflon wrapped scintillator has a 18.2(21) % higher light output compared to a not wrapped scintillator which is in good agreement with the results of other similar experiments [19].

Overall wrapping scintillators in aluminium or teflon is a way to increase the efficiency of a scintillator.

# Chapter 6

## Conclusion

The simulated number of photons is in within one order of magnitude of the measured number which indicates a good correlation between the simulation and the measurement. The impact of surface properties and different wrapping materials was shown and has to be understood and implemented when simulating scintillation light. The advantage of optical coupling with interface pads compared to a direct coupling using no optical interface pads has been shown. Table 6.1 lists the results of the work unless otherwise stated all experiments were carried out using optical interface pads to couple the scintillator and the PMT's.

TABLE 6.1: Overview of the results.

Simulation [ $\gamma$ /Event]	Experiment [ $\gamma$ /Event]	
$244.3 \pm 1.5$	$82.95 \pm 0.25$	simulated for a perfect surface
$151.5 \pm 1.2$	-	simulated for $\sigma$ -alpha of 0.2
-	$70.44 \pm 0.24$	photon yield without OIP
$275.6 \pm 1.6$	$87.17 \pm 0.52$	first geometry, wrapped in Al-foil
$470.8 \pm 2.5$	$84.97 \pm 0.37$	first geometry, wrapped in teflon
$114.94 \pm 0.53$	$86.60 \pm 7.13$	second geometry, unwrapped
$211.64 \pm 0.92$	$102.36 \pm 7.48$	second geometry, wrapped in teflon

The discrepancy in the simulated light yield with a similar energy deposition but a different geometry are intriguing and further investigation in this respect may be needed. In addition it might be necessary to get a closer look at the boundary processes in the simulation for the teflon wrapped scintillator to understand the deviation from the experimental results. The influence of wrapping and geometry of the scintillator on the light guiding properties are not fully understood and might be an interesting topic for further work.

# Bibliography

- [1] S Agostinelli, J Allison, K ea Amako, J Apostolakis, H Araujo, P Arce, M Asai, D Axen, S Banerjee, G Barrand, et al. Geant4—a simulation toolkit. *Nuclear instruments and methods in physics research section A: Accelerators, Spectrometers, Detectors and Associated Equipment*, 506(3):250–303, 2003.
- [2] Q.R. Ahmad et al. Sno collaboration. *Phys. Rev. Lett.* 87, 2001.
- [3] Y. Fukuda et al. Super-kamiokande collaboration. *Phys. Rev. Lett.* 81, 1998.
- [4] K. Eguchi et al. Kamland collaboration. *Phys. Rev. Lett.* 90, 2003.
- [5] A. Blondel, A. Bravar, M. Pohl, S. Bachmann, N. Berger, M. Kiehn, A. Schöning, D. Wiedner, B. Windelband, P. Eckert, H.-C. Schultz-Coulon, W. Shen, P. Fischer, I. Perić, M. Hildebrandt, P.-R. Kettle, A. Papa, S. Ritt, A. Stoykov, G. Dissertori, C. Grab, R. Wallny, R. Gredig, P. Robmann, and U. Straumann. Research proposal for an experiment to search for the decay  $\mu \rightarrow \text{eee}$ . 01 2013. URL <http://arxiv.org/abs/1301.6113>.
- [6] URL [http://aea.web.psi.ch/beam2lines/beam\\_pie5.html](http://aea.web.psi.ch/beam2lines/beam_pie5.html).
- [7] Patrick Eckert, Rainer Stamen, and H-C Schultz-Coulon. Study of the response and photon-counting resolution of silicon photomultipliers using a generic simulation framework. *Journal of Instrumentation*, 7(08):P08011, 2012.
- [8] U.Straumann et al. Search for the rare decay  $\mu+ \rightarrow e^+ e^- e^+$ . *Annual Report Physik Institut Zurich*, 2012/2013.
- [9] Claude Amsler. *Kern- und Teilchenphysik*. vdf, 2007.
- [10] R. Reif D. Seeliger G. Musiol, J. Ranft. *Kern- und Elementarteilchenphysik*. VCH Verlagsgesellschaft, 1988.
- [11] Saint-Gobain Ceramics and Plastics. *BC-400,BC-404,BC-408,BC-412,BC-416*, 2005.
- [12] J. Beringer et al. (Particle Data Group), *Phys. Rev. D86*, 010001 (2012).

- [13] Saint-Gobain Ceramics and Plastics. *Detector Assembly Materials*, 2005.
- [14] Martin Janecek and William W Moses. Simulating scintillator light collection using measured optical reflectance. *Nuclear Science, IEEE Transactions on*, 57(3):964–970, 2010.
- [15] *Geant4 General Particle Source*. <http://reat.space.qinetiq.com/gps/>.
- [16] Rene Brun and Fons Rademakers. Root—an object oriented data analysis framework. *Nuclear Instruments and Methods in Physics Research Section A: Accelerators, Spectrometers, Detectors and Associated Equipment*, 389(1):81–86, 1997.
- [17] Wouter Verkerke and David Kirkby, 2003. URL <http://roofit.sourceforge.net/>.
- [18] *BURLE Electrontubes S83062E*.
- [19] S Scheu, H Kaspar, P Robmann, A van der Schaaf, and P Truöl. Studies on wrapping materials and light collection geometries in plastic scintillators. *Nuclear Instruments and Methods in Physics Research Section A: Accelerators, Spectrometers, Detectors and Associated Equipment*, 567(1):345–349, 2006.